**Supplemental Information**

**Systemic inhibition of PTPN22 augments anticancer immunity**

**Supplemental Figure 1**

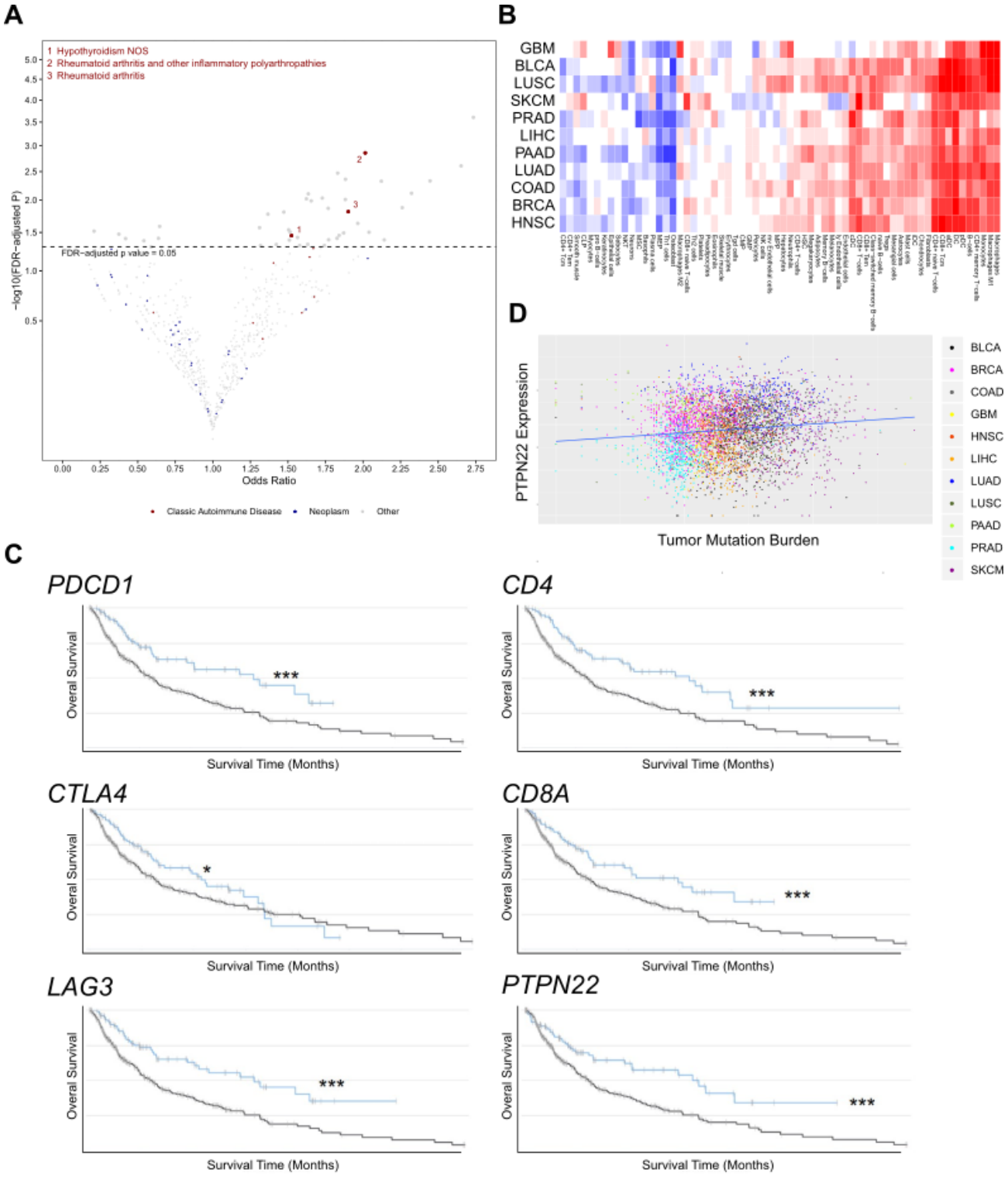


**PTPN22 correlates with negative immune regulation in cancers.** (**A**) A volcano plot of the results from the analysis using phenome-wide association studies (PheWAS) from the Vanderbilt BioVU database focused on de-identified patients of African ancestry. (**B**) A heatmap of correlations between *Ptpn22* expression and several cell type signatures based on a gene set based algorithm, xCell, across 11 cancer types in the Cancer Genome Atlas (TCGA). (**C**) Kaplan-Meier curves represent univariate survival analyses for six genes, *Pdcd1*, *Ctla4*, *Lag3*, *Cd4*, *Cd8a*, and *Ptpn22*, stratifying high-expressor cases (top 20%, blue) vs. the remaining (black) using the melanoma TCGA database. *p<0.05, ***p<0.005, log-rank tests. (**D**) Correlation between the *Ptpn22* expression and the total number of mutations are shown in aggregate for 11 cancer types from TCGA. Blue line represents the overall correlation strength (0.142). Abbreviations: breast cancer, BRCA; head and neck squamous cell cancer, HNSC; hepatocellular carcinoma, LIHC; lung adenocarcinoma, LUAD; lung squamous cell carcinoma, LUSC; pancreatic ductal adenocarcinoma, PAAD; prostate adenocarcinoma, PRAD; skin melanoma, SKCM.

**Supplemental Figure 2**

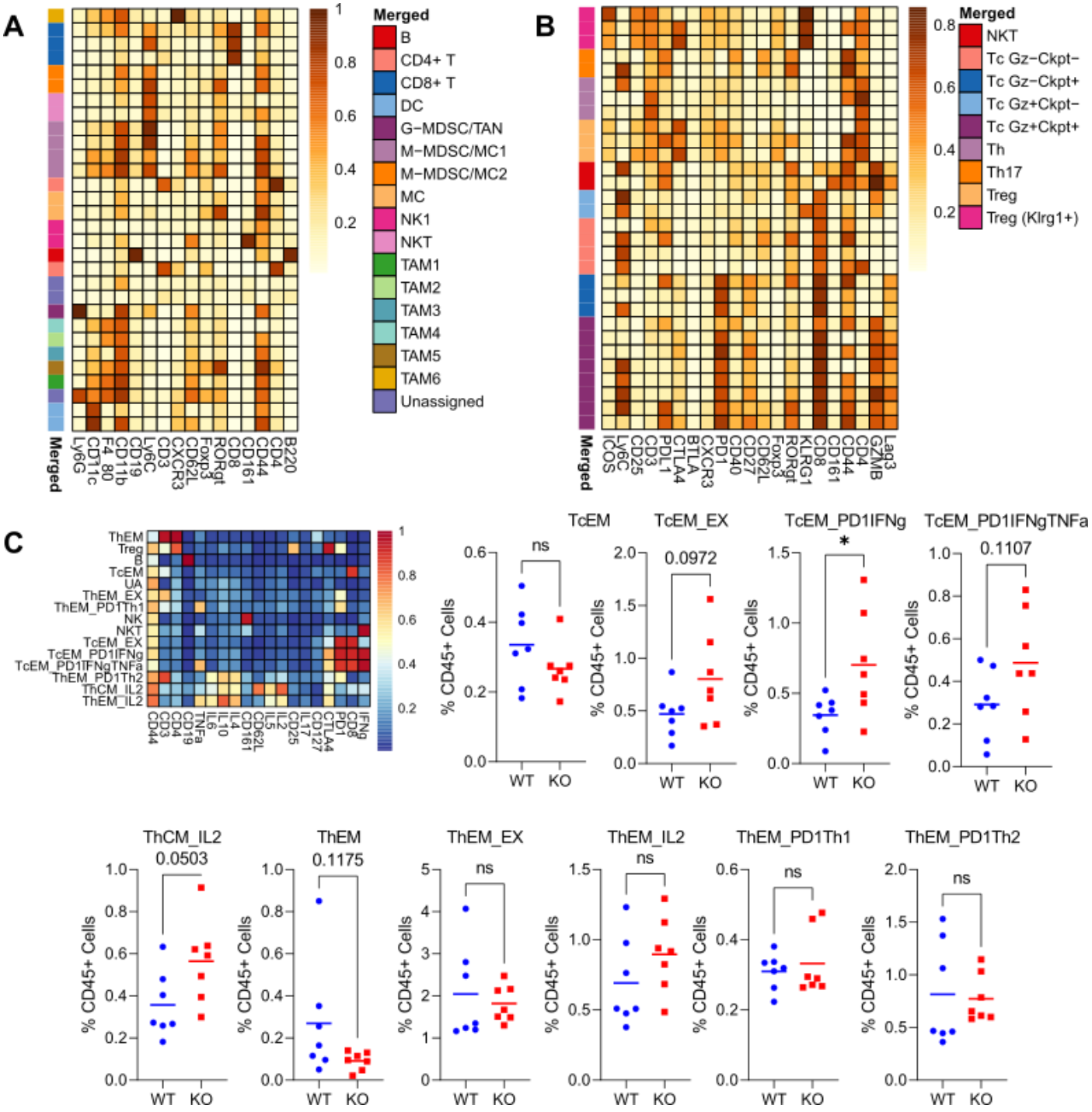


**Analysis of immune profiles within tumors based on CyTOF analysis.** (**A**) CyTOF analysis based on FlowSOM clustering into 30 metaclusters into 16 final major immune cell types for global immune profiling of the tumors is shown as a normalized expression heatmap. (**B**) An in-depth T cell population analysis of the using FlowSOM clustering into 30 metaclusters annotated into 9 final T cell subtypes is shown as a normalized expression heatmap. Clusters annotated in **A** and **B** correspond to the cell types shown on Figure 2. (**C**) Expression heatmap of additional T cell profiling based on cytokine markers using a separate CyTOF panel. Proportion of tumor-infiltrating $CD8^+$ cytotoxic T cell (Tc) and $CD4^+$ helper T cell (Th) subtypes distinguished by cytokine expression are shown as dot plots. *<0.05 by unpaired T-tests (n=7). Abbreviations: Abbreviations: central memory, CM; checkpoint markers, Ckpt; dendritic cells, DC; granulocytic myeloid-derived suppressor cells/tumor associated neutrophils, effector memory, EM; exhaustion markers, EX; G-MDSC/TAN; granzyme, Gz; monocytic myeloid-derived suppressor cells/myeloid cells, M-MDSC/MC; monocytes, MC; natural killer cells, NK; natural killer T cells, NKT; tumor-associated macrophages, TAM; cytotoxic T cells, Tc; helper T cells, Th; regulatory T cells, Treg.

**Supplemental Figure 3**

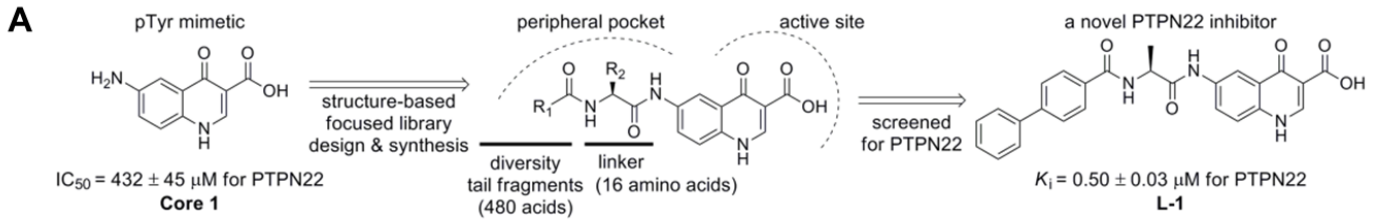


**B**

| PTP | $IC_{50}$ (μM) for L-1 | PTP | $IC_{50}$ (μM) for L-1 |
|---|---|---|---|
| PTPN22 | 1.4 ± 0.2 | PTPε | > 50 |
| PTP1B | > 25 | LAR | > 50 |
| SHP2 | 10.6 ± 0.6 | CD45 | > 25 |
| TC-PTP | > 25 | VHR | 13.9 ± 3.2 |
| PTP-Meg2 | > 50 | VHX | > 25 |
| PTP-PEST | 15.2 ± 2.0 | CDC14 | > 25 |
| PTPD1 | > 50 | Laforin | > 50 |
| PTPα | > 25 | LMWPTP | 11.6 ± 5.2 |
| PTPγ | > 50 | | |

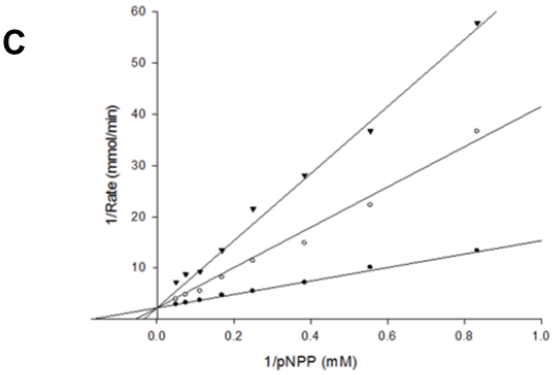


**Synthesis and Characterization of a novel PTPN22 inhibitor, L-1.** (**A**) A quinolone derivative Core 1 with 3-Carboxy-4-quinolone scaffold which is commonly found in drugs and bioactive compounds could serve as a potential novel pTyr mimetic to engage the PTPN22 active site. To increase the potency and selectivity of Core 1 for PTPN22, we aimed to install molecular diversity to Core 1 in order to capture additional and less conserved interactions outside the pTyr-binding cleft (i.e. active site). Preliminary molecular modeling suggested that the carboxylic acid and the quinoline ring occupy the PTPN22 active site and the 6-position amino group is solvent exposed. The positioning of the 6-amino group affords us the opportunity to tether Core 1 to diverse molecular fragments in order to engage unique peripheral pockets in the vicinity of the PTPN22 active site. Based on preliminary modeling, we designed and synthesized a series of bivalent compounds by connecting the 6-amino group of Core 1, via a L-lysine linker, to 480 carboxylic acids that differ in size, polarity, solubility, and drug-like properties ($R_1$). High throughput screening of the fragment-based focused library identified the biphenyl carboxylic acid group as one of the most potent fragments for PTPN22. To optimize the linker interaction with PTPN22, 16 different amino acids with neutral, acidic, and basic side chains ($R_2$) were surveyed to further increase binding affinity, from which a novel PTPN22 inhibitor L-1 was identified. (**B**) To determine the selectivity of L-1 for PTPN22, its inhibitory activity toward a panel of 16 mammalian PTPs were also measured. (**C**) Kinetic analyses showing competitive inhibition of L-1 for PTPN22 with *K*i = 0.50 ± 0.03 μM. (**D**) *In vivo* pharmacokinetics data based on mass spectrometry quantification at 0 h, 1.0 h, 1.5 h, 2.0 h, 2.5 h, 3.0 h, 6.0 h, and 24.0 h from time of intraperitoneal injection of L-1 for three mice are shown.

**Supplemental Figure 4**

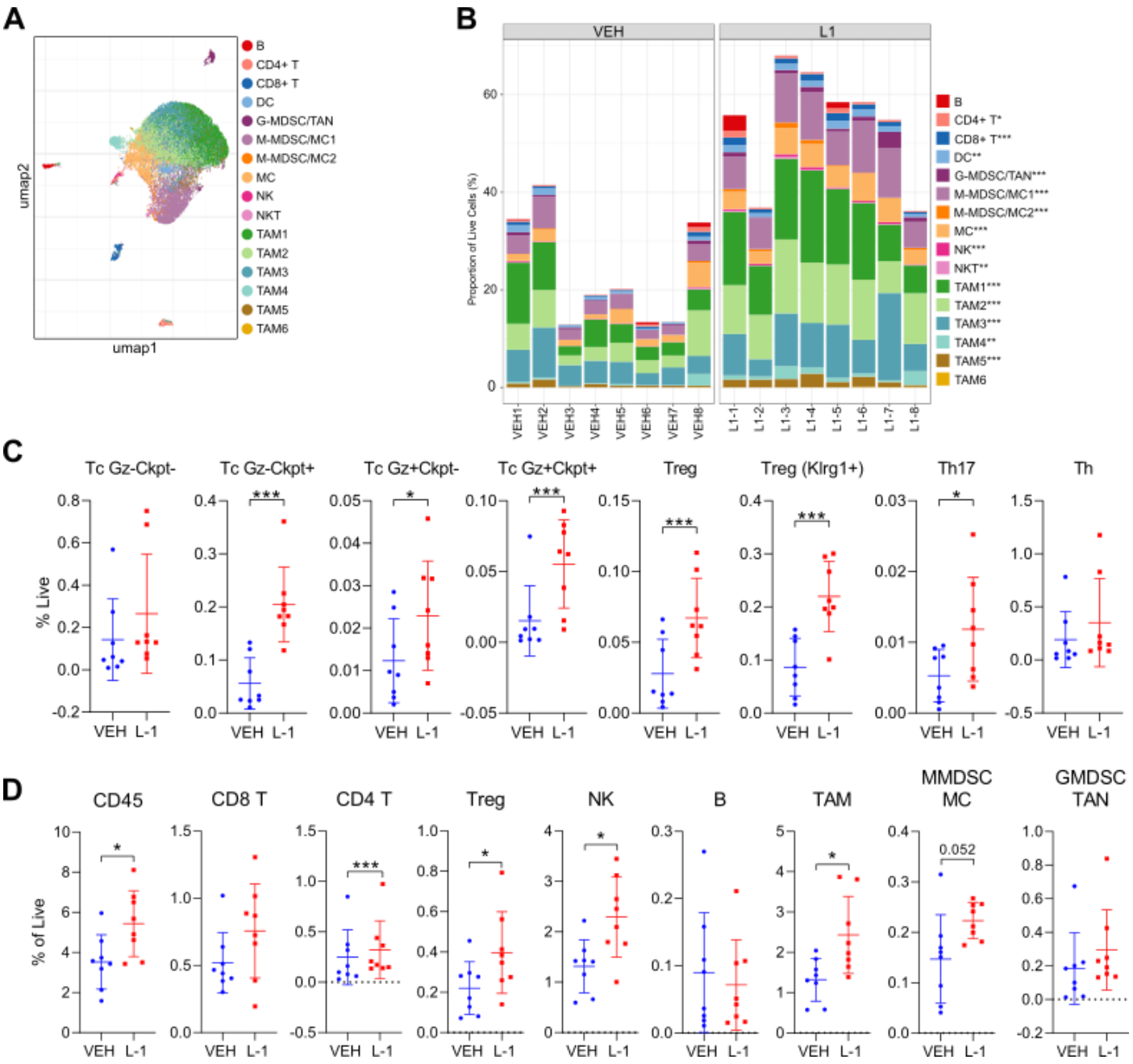


**L-1 augments in vivo antitumor immune responses.** (**A**-**C**), Immune profiles in MC38 tumors treated with vehicle (VEH) or L-1. Resulting UMAP plot (A) from CyTOF analysis of the immune profile. Immune subsets (B) and T cell subsets (C) are represented as percentage of live cells. (**D**) Given relatively low immune cell abundance in CT26 tumors, supervised gating analysis was performed to evaluate immune profiles in CT26 tumors treated with vehicle (VEH) or L-1. Mean + s.e.m., n=8, *p<0.05, **p<0.01, ***p<0.005, results of T-tests paired by batch. Abbreviations: checkpoint markers, Ckpt; dendritic cells, DC; granulocytic myeloid-derived suppressor cells/tumor associated neutrophils, G-MDSC/TAN; granzyme, Gz; monocytic myeloid-derived suppressor cells/myeloid cells, M-MDSC/MC; monocytes, MC; natural killer cells, NK; natural killer T cells, NKT; tumor-associated macrophages, TAM; cytotoxic T cells, Tc; helper T cells, Th; regulatory T cells, Treg.

**Supplemental Figure 5**

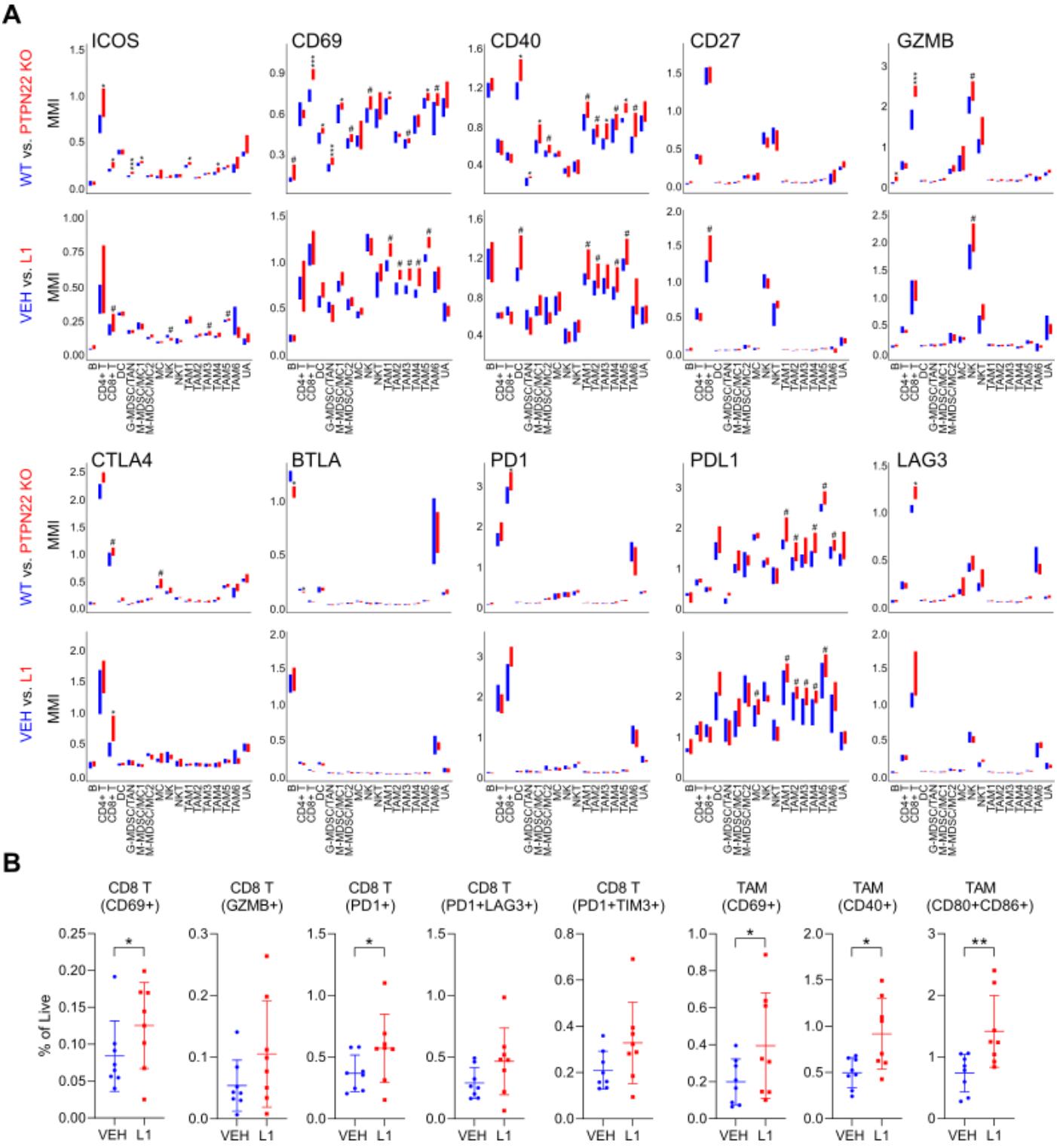


**Abrogation of PTPN22 leads to enhanced activation of T cell and TAMs.** (**A**) Two separate experiments are shown: WT vs. PTPN22 KO and vehicle (VEH) vs. L-1. MC38 tumor-infiltrating immune cells are profiled by CyTOF. Mean metal intensities for each of the functional marker expression stratified by the cell types (n=8). #<0.2, *<0.1, ***<0.005. Abbreviations: dendritic cells, DC; granulocytic myeloid-derived suppressor cells/tumor associated neutrophils, G-MDSC/TAN; granzyme, Gz; monocytic myeloid-derived suppressor cells/myeloid cells, M-MDSC/MC; monocytes, MC; natural killer cells, NK; natural killer T cells, NKT; tumor-associated macrophages, TAM; cytotoxic T cells, Tc; helper T cells, Th; regulatory T cells, Treg; unassigned, UA. (**B**) CT26 tumors treated with VEH or L-1 are profiled by CyTOF to determine the expression of functional markers in $CD8^+$ T cells and TAMs (n=8). *<0.05, **<0.01.

**Supplemental Figure 6**

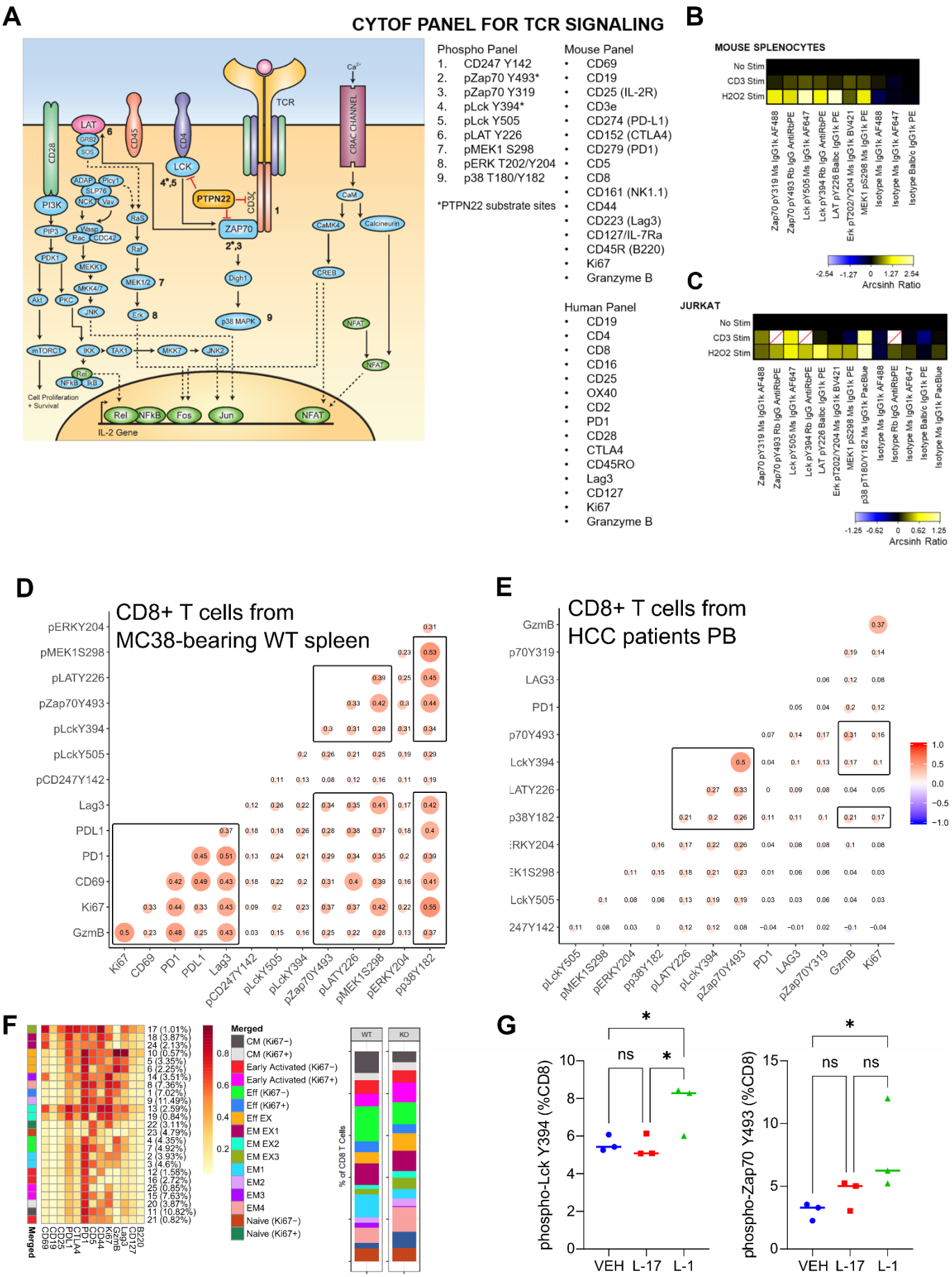


**CyTOF phospho-profiling of CD8 T cells.** (**A**) Design of the CyTOF phospho-profiling panel, denoting 9 phospho-sites along the TCR signaling pathway. Antibodies cross-reactive for both human and mice are used. 15-16 additional subtyping/functional markers are incorporated for the mouse and human panels. (**B**

and **C**) The phospho-specific antibody clones and the phospho-staining protocol are validated using two stimulation conditions, anti-CD3 and hydrogen peroxide (H2O2), in mouse splenocytes and Jurkat E6-1 cells, leading to increased phosphorylation levels compared to the unstimulated condition. Stimulated-to-unstimulated ratios of arcsinh transformed phosphorylation levels are indicated by the color key. Red lines signify untested. (**D** and **E**) Correlation matrices obtained from phospho-profiling $CD8^+$ T cells from spleens of MC38-bearing WT mice (aggregate data from 4 mice) and peripheral blood (PB) of hepatocellular carcinoma (HCC) patients not exposed to immunotherapy (aggregate data from 4 patients). The correlation strengths are indicated by color (positive: red; negative: blue), the size of the circles, and annotated with numbers. Notable correlations are outlined. (**F**) The result from the FlowSOM clustering into 25 metaclusters based on 14 lineage/functional markers and then annotated into 16 final subtypes of $CD8^+$ T cells for phospho-profiling of the tumors is shown as a normalized metal intensity heatmap. Stacked bar graphs represent the $CD8^+$ T cell profile upon clustering and annotation based on the results from the FlowSOM algorithm. Abbreviations: central memory subtype, CM; effector memory subtype, CM; effector subtype, Eff; “exhausted” subtype (positive expression of checkpoint markers), EX. (**G**) Phosphorylation levels of PTPN22-specific sites as a percentage of $CD8^+$ T cells from spleens immediately fixed upon harvest and dissociation from mice treated with vehicle (VEH), a negative compound (L-17), and L-1 via subcutaneous osmotic pumps for 3 days. Dot plots with median bars (n=3). *$p<0.05$, two-tailed t-tests.

**Supplemental Figure 7**

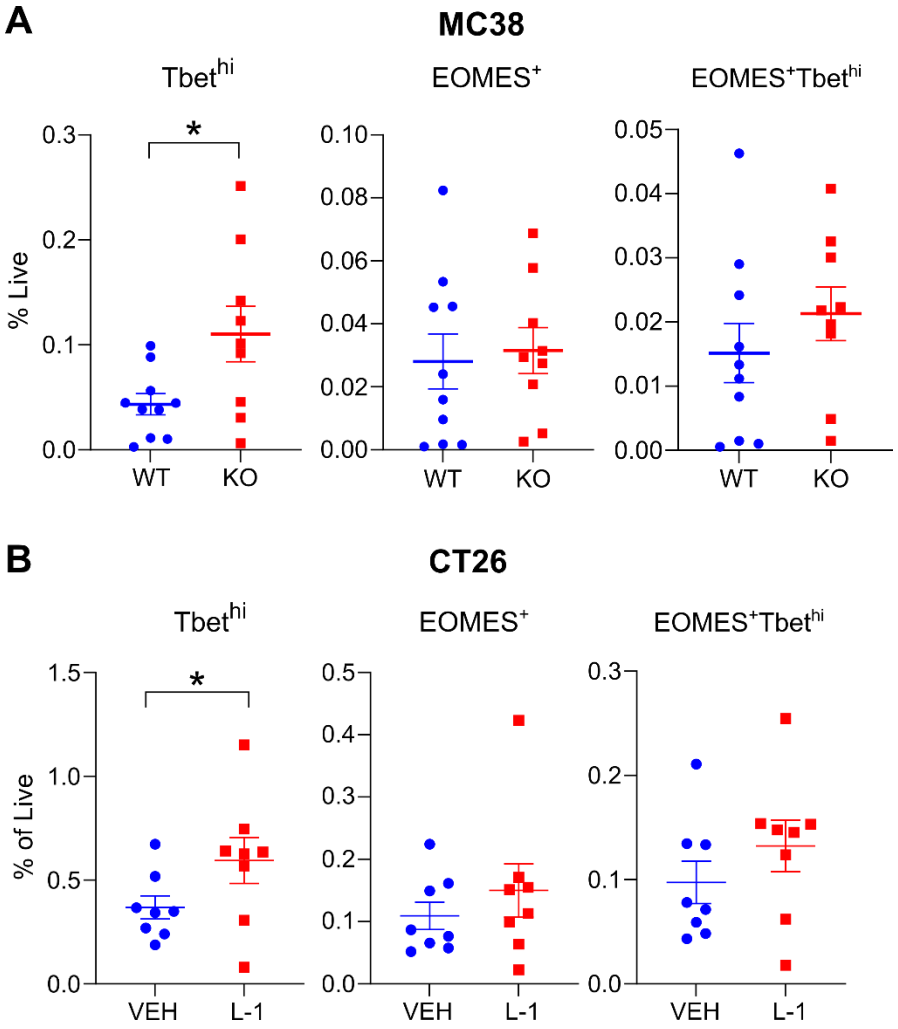


**Tbet and EOMES expression in tumor-infiltrating CD8⁺ T cells.** Dot plots with mean ± s.e.m. (n=9-10) for flow cytometry to determine the proportion of tumor infiltrating CD8+ T cells that are Tbet$^{hi}$, EOMES$^{+}$, and EOMES$^{+}$Tbet$^{hi}$ in the (**A**) MC38 and (**B**) CT26 tumors. *p <0.05, two-tailed unpaired t-test.

**Supplemental Figure 8**

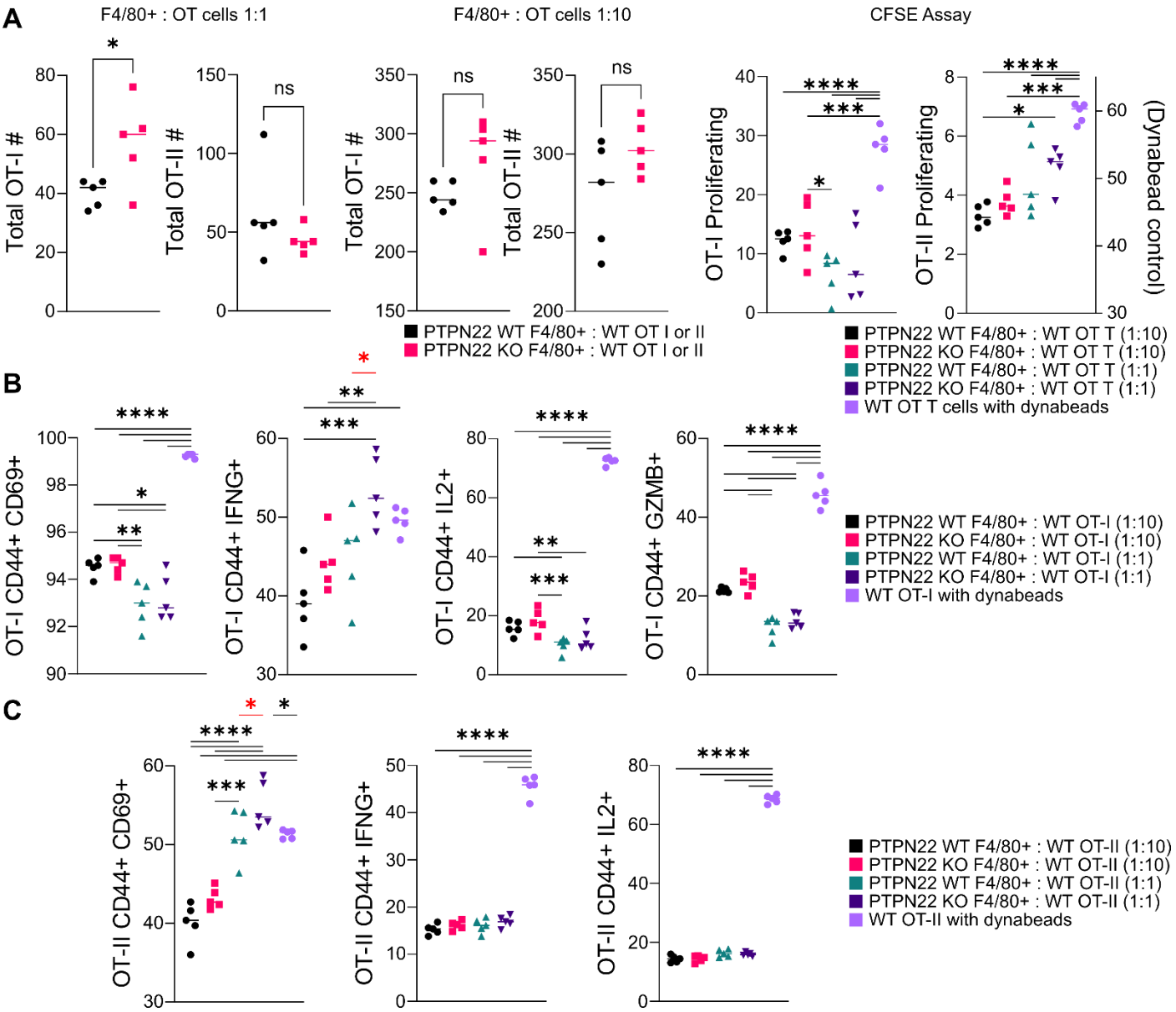


**PTPN22-mediated effects of tumor associated macrophage (TAM) on T cells.** F4/80$^+$ tumor-associated macrophages (TAM) derived from MC38-OVA tumors from either PTPN22 KO or WT mice (n=5) were co-cultured with CD8$^+$ OT-I and CD4$^+$ OT-II T cells enriched from spleens for 72 hours. Co-culturing was done at two different TAM:T cell ratios (1:1 or 1:10). (**A**) Numbers of T cells counted at the end of co-cultures and the results of the CFSE+ assay are shown. (**B** and **C**) CD69, IFN, IL2, or granzyme B expressions were assessed for (**B**) OT-I T cells and (**C**) OT-II T cells using flow cytometry. p-value *<0.05, **<0.01, ***<0.005, ****<0.0001 by unpaired two-tailed t-tests (for T cell numbers) or ANOVA (for marker expressions). Red asterisks mark significant differences between WT and PTPN22 KO TAMs in a given condition.

**Supplemental Figure 9**

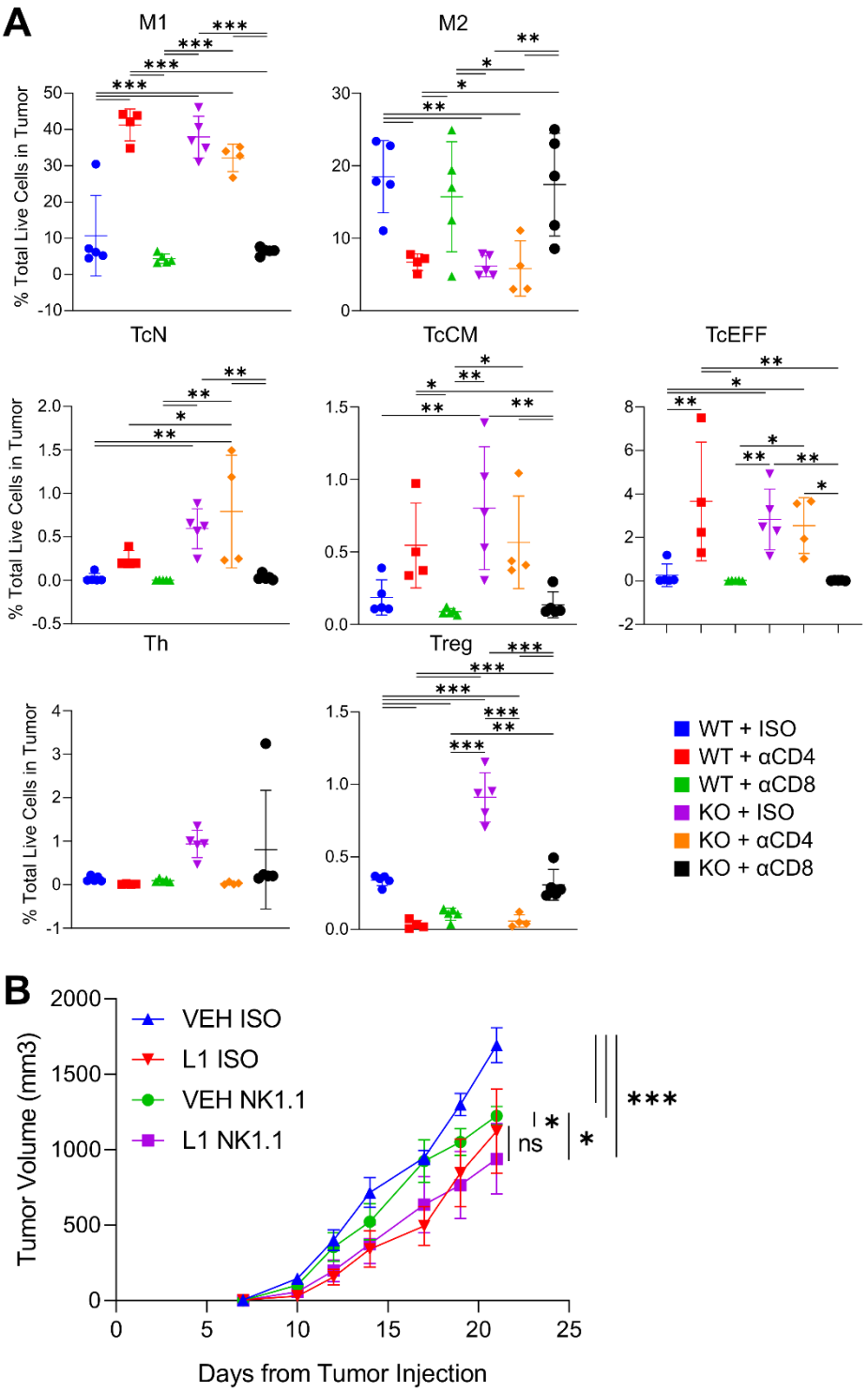


**Effects of CD4, CD8, or NK1.1. depletion in the MC38 model.** (**A**) Abundances of immune cells in MC38 tumors from WT or PTPN22 KO mice treated with isotype, anti-CD4, or anti-CD8 antibodies for depletion as a result of CyTOF profiling (n=4-5, mean±S.D.). p-values: *0.05, **<0.01, ***<0.005 by ANOVA, adjusted for FDR. Abbreviations: central memory, CM; EFF, effector; M1-like TAM, M1; M2-like TAM, M2; naïve, N; Tc; helper T cells, Th; regulatory T cells, Treg. (**B**) Effects of VEH vs. L-1 with isotype (ISO) or anti-NK1.1 antibody on MC38 tumor growth are shown (n=5). p-values: *<0.05, ***<0.005, nonlinear regression.

**Supplemental Methods: Patient Cohort Study using BioVU Database**

A retrospective case-controlled study using Electronic Health Records (EHR) within the Vanderbilt University Medical Center "Synthetic Derivative" (SD) and BioVU database was carried out to determine the utility of the PTPN22 SNP variant Rs2476601 as a predictive biomarker for response to single agent immunotherapy. The SD is a de-identified copy of the main hospital medical record databases created for research purposes. The de-identification of SD records was achieved primarily through the application of a commercial electronic program, which was applied and assessed for acceptable effectiveness in scrubbing identifiers. The SD database (which contains over 1.5 million electronic records, with no defined exclusions) was accessed through database queries and search queries based on patient inclusion criteria. Genetic data is integrated with the SD through the BioVU database. The primary outcome of the study was progression free survival (PFS). Eligible patients were selected based on the availability of genotype data for rs2476601 within the BioVu database (n=86,479). Patients selected for the study contained at least one PheCode (phenotypic codes used in SD) for neoplasm, regardless of tissue type, and with mention of at least one of the following immunotherapy checkpoint inhibitors; Ipilimumab, Pembrolizumab, Nivolumab, Atezolizumab, Durvalumab (n = 606), within their EHR. There was no restriction regarding age, race, ethnicity, or gender. Eligible patients for case selection contained the rs2476601 PTPN22 variant and may be heterozygous or homozygous for the variant. Patients were stratified for single agent (n = 51) or combination therapy (n=17). Patients that did not contain the rs2476601 PTPN22 variant or any other alteration within the PTPN22 gene were used as controls. Due to the significantly larger sample size of the WT control arm, a case-control study design was implemented to maintain equal stratification of single agent and combination therapy cases across both arms. Blind selection of control patients was carried out and case-matched. Within the control arm, 92 patients were blindly selected and screened to obtain 51 single agent therapy cases, 9 combination therapy cases, and 32 cases with not enough information. To maintain equivalent sample sizes across treatment arms, an additional 52 patients were blind selected and screened for cases of combination therapy only (n=9). This is summarized in Supplemental Methods Figure 1. Retrospective chart analysis was used to determine PFS from start of specified immunotherapy to time of progression based on scan dates and physician remarks. Statistical significance was determined using the log-rank (Mantel-Cox) test via GraphPad Prism 8.0 Software.

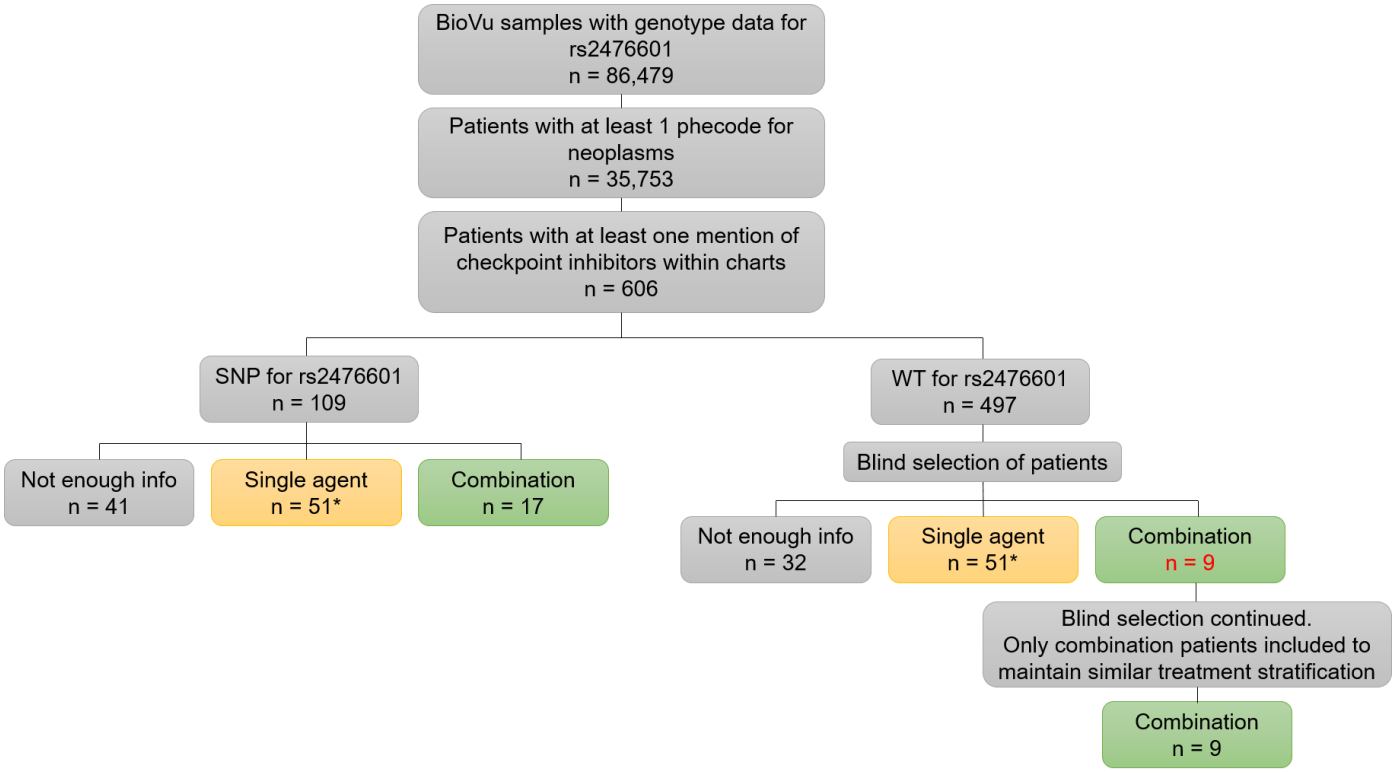


Supplemental Methods Figure 1. Case Controlled Study Design

## Supplemental Methods: Synthesis and Characterization of Novel Inhibitors of PTPN22

### General synthetic procedures and reagents.

Unless otherwise specified, all reagents were purchased from commercial suppliers and used directly without further purification. Analytical thin layer chromatography (TLC) was performed on 0.25 mm silica gel 60-$F_{254}$. Column chromatography was performed using KP-SIL silica gel (Biotage, USA), and flash column chromatography was performed on Biotage prepacked columns using the automated flash chromatography system Biotage Isolera One. The $^{1}H$ and $^{13}C$ NMR spectra were recorded on a Bruker AVANCE 500 MHz instrument. Chemical shifts for Proton magnetic resonance spectra ($^{1}H$ NMR) were quoted in parts per million (ppm) referenced to the appropriate solvent peak or 0.0 ppm for tetramethylsilane (TMS). The following abbreviations were used to describe peak splitting patterns when appropriate: br = broad, s = singlet, d = doublet, t = triplet, q = quartet, m = multriplet, dd = doublet of doublet. Coupling constants, J, were reported in hertz unit (Hz). Chemical shifts for 13C NMR were reported in ppm referenced to the center line at 39.52 of DMSO-d. Low-resolution mass spectra and purity data were obtained using an Agilent Technologies 6470 series, triple quadrupole LC/MS. High-resolution mass spectra (HRMS) were recorded on an Agilent Mass spectrometer using ESI-TOF (electrospray ionization-time of flight).

### Synthesis of Compound L-1

Starting from *p*-nitroaniline (**2**) and diethyl ethoxymethylenemalonate (**3**), advanced intermediate ethyl 6-nitro-4-oxo-1,4-dihydroquinoline-3-carboxylate (**4**) was obtained following a previously reported protocol[1]. The intermediate was then hydrogenated by Pd/C and $H_2$ to provided compound **(5)** in good yield. Condensation of compound (**5**) with Fmoc-L-Ala-OH in the presence of HOBt, HBTU and DIPEA in DMF gave the Fmoc-protected intermediate (**6**). Deprotection of the Fmoc group was carried by using 20% piperidine containing DMF solution at room temperature. Compound (8) was obtained by condensing compound (**7**) with biphenyl-4-carboxylic acid in similar reaction condition as the previous condensation reaction. Final hydrolyzation using aq KOH in a mixture of MeOH/$H_2O$ afforded high yield of **L-1** as free acid after acidification by aq HCl.

**Scheme 1.** Synthesis of Compound L-1[a]

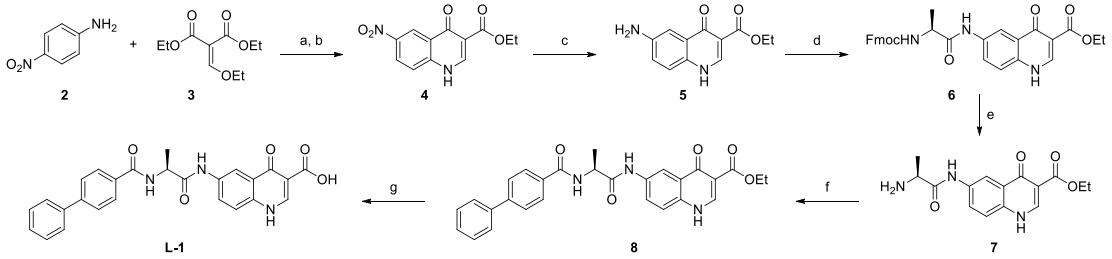


[a]Reagents and conditions: (a) 135°C, 2 h, 75%; (b) PhOPh, reflux, 1 h, 95%; (c) Pd/C, $H_2$, DMF, 100°C, 12 h, 85%; (d) Fmoc-L-Ala-OH, HOBt, HBTU, DIPEA, DMF, r.t., overnight, 65%; (e) Piperidine, DMF, r.t., 1 h, 69%; (f) Biphenyl-4-carboxylic acid, HOBt, HBTU, DIPEA, DMF, r.t., overnight, 78%; (g) KOH, MeOH/$H_2O$, 60°C, 16 h, 90%.

*6-amino-4-oxo-1,4-dihydroquinoline-3-carboxylic acid (**Core 1**).*

Purchased from Princeton BioMolecular Research, Inc. as pale yellow solid. $^{1}H$ NMR (500 MHz, DMSO) $\delta$ 15.99 (s, 1H), 13.12 (brs, 1H), 8.60 (s, 1H), 7.55 (d, $J$ = 8.8 Hz, 1H), 7.32 (d, $J$ = 2.6 Hz, 1H), 7.18 (dd, $J$ = 2.6, 8.8 Hz, 1H), 5.79 (s, 1H); LC-MS (ESI): 205.0 $(M + H)^+$, 203.0 $(M - H)^-$; HRMS (ESI-TOF): m/z $[M - H]^-$ calculated for $C_{10}H_7N_2O_3$: 203.0462, found: 203.0461; Purity: >95% (UV, λ = 254 nm).

*ethyl 6-amino-4-oxo-1,4-dihydroquinoline-3-carboxylate (**5**).*

To a solution of 6-nitro-4-oxo-1,4-dihydroquinoline-3-carboxylate (2.0 g, 7.63 mmol) in dimethylformamide (DMF, 40 ml), was added 10% Pd/C (0.2 g). Hydrogenation was carried out under a pressure of 1 atm at 100°C. After stirring for 12 hours, removal of the catalyst and solvent gave a solid residue, which was then washed by ethyl acetate (40 ml) to afford ethyl 6-amino-4-oxo-1,4-dihydroquinoline-3-carboxylate (1.5 g, 85% yield). $^{1}H$ NMR (500 MHz, DMSO) δ 12.03 (s, 1H), 8.32 (s, 1H), 7.33 (d, $J$ = 8.7 Hz, 1H), 7.26 (d, $J$ = 2.6 Hz, 1H), 6.99 (dd, $J$ = 8.7, 2.6 Hz, 1H), 5.45 (s, 2H), 4.18 (q, $J$ = 7.1 Hz, 2H), 1.26 (t, $J$ = 7.1 Hz, 3H). LC-MS (ESI): m/z $[M + H]^+$ calcd. For $C_{12}H_{13}N_2O_3$: 233.09, found: 233.10.

*(S)-ethyl 6-(2-((((9H-fluoren-9-yl)methoxy)carbonyl)amino)propanamido)-4-oxo-1,4-dihydroquinoline-3-carboxylate (**6**).*

Fmoc-L-Ala-OH (2.0 g, 6.42 mmol), HOBt (1.13 g, 8.35 mmol) and HBTU (3.17 g, 8.35 mmol) were dissolved in dry dimethylformamide (DMF, 40 ml). The mixture was stirred at room temperature for 15min.

Ethyl 6-amino-4-oxo-1,4-dihydroquinoline-3-carboxylate (1.34 g, 5.78 mmol) and N,N-Diisopropylethylamine (3.4 ml, 19.27 mmol) were then added and the resulting mixture was stirred at room temperature over night. DMF was removed by rotary evaporator, Ethyl acetate and water were then added. The formed precipitate was collected by filtration and purified by column chromatography eluting with dichloromethane/methanol 10:1 v/v to give the Fmoc-protected intermediate (**5**) as a light brown solid (2.2 g, 65% yield). 1H NMR (500 MHz, DMSO) δ 12.28 (d, *J* = 6.4 Hz, 1H), 10.27 (s, 1H), 8.47 (d, *J* = 6.5 Hz, 1H), 8.39 (d, *J* = 2.1 Hz, 1H), 7.95 (dd, *J* = 8.9, 2.3 Hz, 1H), 7.88 (d, *J* = 7.6 Hz, 2H), 7.75 – 7.68 (m, 3H), 7.57 (d, *J* = 8.9 Hz, 1H), 7.44 – 7.37 (m, 2H), 7.35 – 7.28 (m, 2H), 4.28 – 4.26 (m, 2H), 4.21 – 4.17 (m, 4H), 1.32 (d, *J* = 7.1 Hz, 3H), 1.26 (t, *J* = 7.1 Hz, 3H). LC-MS (ESI): m/z $[M + H]^+$ calcd. For $C_{30}H_{28}N_3O_6$: 526.20, found: 526.30.

*(S)-ethyl 6-(2-aminopropanamido)-4-oxo-1,4-dihydroquinoline-3-carboxylate (**7**)*.

The Fmoc-protected intermediate **6** (2.1 g, 4.0 mmol) was dissolved in DMF (30 ml). Piperidine (7.5 ml) was added and the reaction mixture stirred at room temperature for 1 hour. Concentration in vacuo gave a brown solid which was washed by ethyl acetate to afford the title compound (0.83 g, 69% yield). $^1$H NMR (500 MHz, DMSO) δ 8.49 (s, 1H), 8.43 (d, *J* = 2.4 Hz, 1H), 7.98 (dd, *J* = 8.9, 2.4 Hz, 1H), 7.58 (d, *J* = 8.9 Hz, 1H), 4.21 (q, *J* = 7.1 Hz, 2H), 3.52 – 3.47 (m, 1H), 1.27 (t, *J* = 7.1 Hz, 3H), 1.25 (d, *J* = 6.9 Hz, 3H). LC-MS (ESI): m/z $[M + H]^+$ calcd. For $C_{15}H_{18}N_3O_4$: 304.13, found: 304.20.

*(S)-ethyl 6-(2-([1,1'-biphenyl]-4-ylcarboxamido)propanamido)-4-oxo-1,4-dihydroquinoline-3-carboxylate (**8**)*.

Biphenyl-4-carboxylic acid (0.40 g, 2.02 mmol), HOBt (0.35 g, 2.62 mmol) and HBTU (1.0 g, 2.62 mmol) were dissolved in dry dimethylformamide (DMF, 20 ml). The mixture was stirred at room temperature for 15min. (S)-ethyl 6-(2-aminopropanamido)-4-oxo-1,4-dihydroquinoline-3-carboxylate (0.55 g, 1.82 mmol) and N,N-Diisopropylethylamine (1.07 ml, 6.05 mmol) were then added and the resulting mixture was stirred at room temperature over night. DMF was removed by rotary evaporator, Ethyl acetate and water were then added. The formed precipitate was collected by filtration and washed by ethyl acetate to give (S)-ethyl 6-(2-([1,1'-biphenyl]-4-ylcarboxamido)propanamido)-4-oxo-1,4-dihydroquinoline-3-carboxylate (0.76 g, 78% yield). $^1$H NMR (500 MHz, DMSO) δ 12.30 (d, *J* = 6.7 Hz, 1H), 10.36 (s, 1H), 8.74 (d, *J* = 7.0 Hz, 1H), 8.48 (d, *J* = 6.7 Hz, 1H), 8.41 (d, *J* = 2.3 Hz, 1H), 8.03 (d, *J* = 8.4 Hz, 2H), 8.00 (dd, *J* = 8.9, 2.4 Hz, 1H), 7.79 (d, *J* = 8.4 Hz, 2H), 7.75 (d, *J* = 7.2 Hz, 2H), 7.59 (d, *J* = 8.9 Hz, 1H), 7.50 (t, *J* = 7.6 Hz, 2H), 7.41 (t, *J* = 7.4 Hz, 1H), 4.67 – 4.61 (m, 1H), 4.21 (q, *J* = 7.1 Hz, 2H), 1.48 (d, *J* = 7.2 Hz, 3H), 1.28 (t, *J* = 7.1 Hz, 3H). LC-MS (ESI): m/z $[M + H]^+$ calcd. For $C_{28}H_{26}N_3O_5$: 484.19, found: 484.20.

*(S)-6-(2-([1,1'-biphenyl]-4-ylcarboxamido)propanamido)-4-oxo-1,4-dihydroquinoline-3-carboxylic acid (**L-1**).*

To a solution of compound **8** (500 mg, 1.03 mmol) in Methanol (20 ml) and $H_2O$ (20 ml), KOH (580 mg, 10.34 mmol) was added. The obtained mixture was stirred at 60°C for 16 hours. The mixture was brought to 0°C, carefully acidified with 1N HCl until pH = 1. The formed precipitate was collected by filtration and purified by HPLC to furnish the desired product **L-1** as an off-white solid (422 mg, 90% yield). $^1$H NMR (500 MHz, DMSO) δ 10.53 (s, 1H), 8.83 (d, *J* = 6.8 Hz, 1H), 8.78 (d, *J* = 6.8 Hz, 1H), 8.65 (d, *J* = 2.4 Hz, 1H), 8.10 (dd, *J* = 9.1, 2.4 Hz, 1H), 8.04 (d, *J* = 8.5 Hz, 2H), 7.84 – 7.77 (m, 3H), 7.76 – 7.70 (m, 2H), 7.50 (t, *J* = 7.6 Hz, 2H), 7.45 – 7.39 (m, 1H), 4.68 – 4.61 (m, 1H), 1.49 (d, *J* = 7.2 Hz, 3H). $^{13}$C NMR (126 MHz, DMSO) δ 177.99 (s), 172.03 (s), 166.55 (s), 166.08 (s), 144.05 (s), 142.89 (s), 139.15 (s), 137.34 (s), 135.40 (s), 132.67 (s), 129.04 (s), 128.30 (s), 128.08 (s), 126.88 (s), 126.41 (s), 126.19 (s), 124.95 (s), 120.41 (s), 113.21 (s), 107.07 (s), 50.13 (s), 17.61 (s). LC-MS (ESI): m/z $[M - H]^-$ calcd. For $C_{26}H_{20}N_3O_5$: 454.14, found: 454.30. HRMS (ESI-TOF): m/z $[M - H]^-$ calcd. For $C_{26}H_{20}N_3O_5$: 454.1403, found: 454.1413; Purity: >95% (UV, λ = 254 nm).

**Synthesis of Compound L-17**

Starting from 6-aminoquinolin-4(1H)-one (**9**) and Fmoc-L-Ala-OH, the condensation reaction gave the Fmoc-protected intermediate (**10**) in the presence of HOBt, HBTU and DIPEA in DMF. Deprotection of the Fmoc group was carried by using 20% piperidine containing DMF solution at room temperature. Final compound (**L-17**) was obtained by condensing compound (**11**) with biphenyl-4-carboxylic acid in similar reaction condition as the previous condensation reaction.

**Scheme 2.** Synthesis of Compound L-17[a]

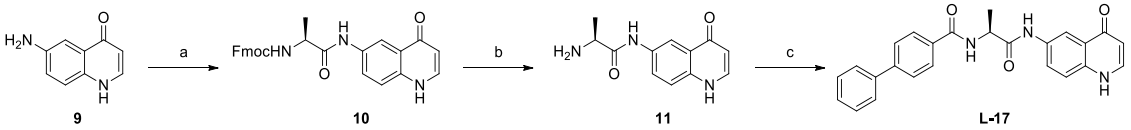


[a]Reagents and conditions: (a) Fmoc-L-Ala-OH, HOBt, HBTU, DIPEA, DMF, r.t., overnight, 87%; (b) Piperidine, DMF, r.t., 1 h, 76%; (c) Biphenyl-4-carboxylic acid, HOBt, HBTU, DIPEA, DMF, r.t., overnight, 71%.

*(S)-(9H-fluoren-9-yl)methyl (1-oxo-1-((4-oxo-1,4-dihydroquinolin-6-yl)amino)propan-2-yl)carbamate (**10**)*.
Fmoc-L-Ala-OH (0.7 g, 2.25 mmol), HOBt (0.39 g, 2.92 mmol) and HBTU (1.11 g, 2.92 mmol) were dissolved in dry dimethylformamide (DMF, 15 ml). The mixture was stirred at room temperature for 15min. 6-Aminoquinolin-4(1H)-one (0.32 g, 2.00 mmol) and N,N-Diisopropylethylamine (1.2 ml, 6.75 mmol) were then added and the resulting mixture was stirred at room temperature over night. DMF was removed by rotary evaporator, Ethyl acetate and water were then added. The formed precipitate was collected by filtration and purified by column chromatography eluting with dichloromethane/methanol 10:1 v/v to give the Fmoc-protected intermediate (**10**) as a light brown solid (0.89 g, 87% yield). $^1$H NMR (500 MHz, DMSO) δ 8.32 (d, *J* = 21.3 Hz, 1H), 7.91 – 7.85 (m, 3H), 7.84– 7.77 (m, 3H), 7.76 – 7.70 (m, 1H), 7.50 (dd, *J* = 8.7, 2.6 Hz, 1H), 7.40 (t, *J* = 7.4 Hz, 2H), 7.33 (t, *J* = 7.4 Hz, 2H), 6.26 (s, 2H), 5.98 – 5.94 (m, 1H), 3.42 (q, *J* = 6.9 Hz, 1H), 1.21 (d, *J* = 6.9 Hz, 3H). LC-MS (ESI): m/z $[M + H]^+$ calcd. For $C_{27}H_{23}N_3O_4$: 454.18, found: 454.30.

*(S)-2-amino-N-(4-oxo-1,4-dihydroquinolin-6-yl)propanamide (**11**)*.
The Fmoc-protected intermediate **10** (0.8 g, 1.76 mmol) was dissolved in DMF (16 ml). Piperidine (4 ml) was added and the reaction mixture stirred at room temperature for 1 hour. Concentration in vacuo gave a brown solid which was washed by ethyl acetate to afford the title compound (0.31 g, 76% yield). $^1$H NMR (500 MHz, DMSO) δ 8.34 (d, *J* = 2.4 Hz, 1H), 7.89 (dd, *J* = 8.9, 2.5 Hz, 1H), 7.82 (d, *J* = 7.3 Hz, 1H), 7.48 (d, *J* = 8.9 Hz, 1H), 5.96 (d, *J* = 7.3 Hz, 1H), 3.42 (q, *J* = 6.9 Hz, 1H), 1.21 (d, *J* = 6.9 Hz, 3H). LC-MS (ESI): m/z $[M + H]^+$ calcd. For $C_{12}H_{14}N_3O_2$: 232.11, found: 232.20.

*(S)-N-(1-oxo-1-((4-oxo-1,4-dihydroquinolin-6-yl)amino)propan-2-yl)-[1,1'-biphenyl]-4-carboxamide (**L-17**)*.
Biphenyl-4-carboxylic acid (0.15 g, 0.76 mmol), HOBt (0.12 g, 0.91 mmol) and HBTU (0.34 g, 0.91 mmol) were dissolved in dry dimethylformamide (DMF, 8 ml). The mixture was stirred at room temperature for 15min. (S)-2-amino-N-(4-oxo-1,4-dihydroquinolin-6-yl)propanamide (0.17 g, 0.75 mmol) and DIPEA (0.40 ml, 2.27 mmol) were then added and the resulting mixture was stirred at room temperature over night. DMF was removed by rotary evaporator, Ethyl acetate and water were then added. The formed precipitate was collected by filtration and washed by ethyl acetate to give (S)-N-(1-oxo-1-((4-oxo-1,4-dihydroquinolin-6-yl)amino)propan-2-yl)-[1,1'-biphenyl]-4-carboxamide (0.22 g, 71% yield). $^1$H NMR (500 MHz, DMSO) δ 11.73 (d, *J* = 4.9 Hz, 1H), 10.23 (s, 1H), 8.71 (d, *J* = 6.9 Hz, 1H), 8.34 (d, *J* = 2.2 Hz, 1H), 8.02 (d, *J* = 8.3 Hz, 2H), 7.90 (dd, *J* = 9.0, 2.3 Hz, 1H), 7.86 – 7.80 (m, 1H), 7.77 (d, *J* = 8.3 Hz, 2H), 7.73 (d, *J* = 7.4 Hz, 2H), 7.52 – 7.46 (m, 3H), 7.39 (t, *J* = 7.3 Hz, 1H), 5.97 (d, *J* = 7.3 Hz, 1H), 4.62 (p, *J* = 7.1 Hz, 1H), 1.46 (d, *J* = 7.2 Hz, 3H). $^{13}$C NMR (126 MHz, DMSO) δ 177.04 (s), 171.99 (s), 166.49 (s), 143.31 (s), 139.63 (s), 139.29 (s), 136.66 (s), 135.16 (s), 133.23 (s), 129.51 (s), 128.76 (s), 128.54 (s), 127.35 (s), 126.87 (s), 126.60 (s), 124.87 (s), 119.23 (s), 114.49 (s), 108.38 (s), 50.48 (s), 18.24 (s). LC-MS (ESI): m/z $[M + H]^+$ calcd. For $C_{25}H_{22}N_3O_3$: 412.17, found: 412.30.

**Enzyme Kinetic Assay.**

PTP activity was assayed using *p*-nitrophenyl phosphate (*p*NPP) as a substrate in 3,3-dimethylglutarate buffer (50 mM 3,3-dimethylglutarate, pH 7.0, 1 mM EDTA, 150 mM NaCl) at 25 °C. The assays were performed in 96-well plates. Normally, to determine the $IC_{50}$ values for PTPN22, the reaction was initiated by the addition of enzyme (final concentration at 20 nM) to a reaction mixture (final volume 0.2 mL) containing 5.0 mM (Km for the substrate against PTPN22) *p*NPP with serial dilutions. To determine the $IC_{50}$ values for other PTPs, the assays were carried out under the same conditions used for PTPN22 except that the concentration of the *p*NPP was set at the corresponding Km value for each PTP. All PTPs used in the study were recombinant proteins prepared in-house. Concentration of compounds used to determine $IC_{50}$ values ranged from 0.2- to 5-fold of the $IC_{50}$ values. The reaction rate was measured using a SpectraMax Plus 384 microplate spectrophotometer (Molecular Devices). To determine the mode of inhibition, the reactions were initiated by the addition of PTPN22 (final concentration at 20 nM) to the reaction mixtures (0.2 mL) containing various concentrations of *p*NPP and inhibitor **L-1**. Data were fitted using SigmaPlot Enzyme Kinetics Module (Systat Software, Inc.).

**Pharmacokinetics study for L-1**

**L-1** is a novel PTPN22 inhibitor with $IC_{50}$ as low as 1.4 ± 0.2 μM. In order to study the effects of **L-1** in mouse model, pharmacokinetics data is required to understand its absorbance/distribution/metabolism/elimination (ADME) properties. The detailed experimental procedures and resulting pharmacokinetics parameters are present below.

Animal dosing and sample collection for pharmacokinetic studies.

The compound **L-1** was first dissolved in DMSO to make a 20 mg/ml solution. Then the solution was further diluted to a 2 mg/ml solution for which the formulation is 10% DMSO - 85% PBS - 5% Cremophor EL (CrEL). Each mouse was administered a single *IP* dose of 10 mg/kg. The volume of each injection was about 100 μL according to the weigh of mouse. At different time points (1 h, 1.5h, 2 h, 2.5h, 3 h, 6, 24 h), blood samples (50 μL) were collected and centrifuged to get the serum. The serum (10 μL) were then mixed with acetonitrile (20 μL) and centrifuged. The supernatant were collected and subjected to Liquid Chromatography/Mass Spectrometry analysis.

Liquid Chromatography/Mass Spectrometry analysis.

The Liquid Chromatography/Mass Spectrometry (LC/MS) analysis was carried out on a Agilent 1260 analytic HPLC system and an Agilent 6470 Triple Quadrupole MS detector, equipped with a Kinetex 2.6um C18 column (3 mm X 50 mm), eluted with 0-100% MeOH-$H_2O$ with 0.1% (w/v) formic acid at 0.7 mL/min flow-rate (gradient method: 1.2 min 0-10% MeOH linear gradient, 1.5 min 10-90% MeOH linear gradient, followed by 1.3 min 90-100% MeOH, followed by 2.5 min 100% MeOH), MS detector were set at single ion mode (SIM), monitoring the negative charge 454.2 (M-1). The calibration curve of compound **L-1** is shown in Supplemental Methods Figure 2. The detection limit for compound **L-1** is 100 nM at 4 μL sample injection.

Data analysis

The pharmacokinetic parameters were calculated in GraphPad Prism 6, and the results are shown in Supplemental Methods Table 1. The pharmacokinetic curve for compound **L-1** are shown in Supplementary Figure 3.

Supplemental Methods Table 1. The Pharmacokinetic Data for the Compound L-1.

| **Mouse** | **Conc.** | **formulation** | **IP dose** | $C_{max}$ **(μM)** | $t_{max}$ **(h)** | $k_e$ | $t_{1/2}$ **(h)** |
|---|---|---|---|---|---|---|---|
| **#1** | 2 mg/ml | 10% DMSO - 85% PBS - 5% CrEL | 10 mg/kg | 1.31 | 1.5 | 0.583 | 1.189 |
| **#2** | 2 mg/ml | 10% DMSO - 85% PBS - 5% CrEL | 10 mg/kg | 1.09 | 2 | 0.259 | 2.681 |
| **#3** | 2 mg/ml | 10% DMSO - 85% PBS - 5% CrEL | 10 mg/kg | 1.12 | 2 | 0.285 | 2.428 |
| **Average** | 2 mg/ml | 10% DMSO - 85% PBS - 5% CrEL | 10 mg/kg | 1.11 | 2 | 0.341 | 2.031 |

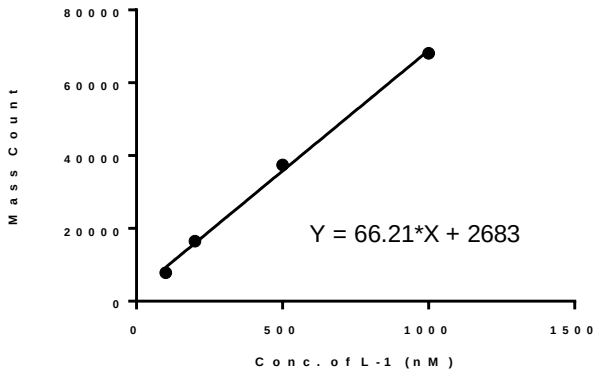


Supplemental Methods Figure 2. The calibration curve for the compound L-1.

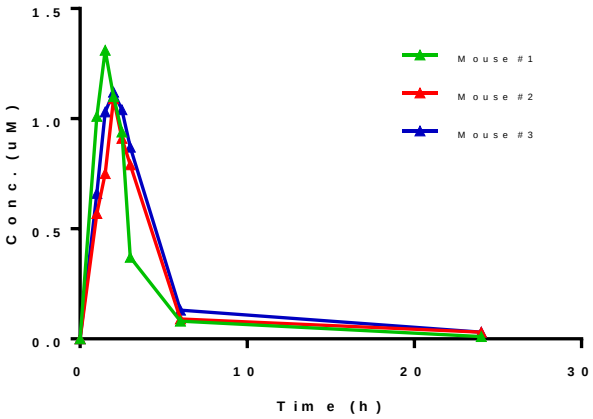


Supplemental Methods Figure 3. The pharmacokinetic data for the compound L-1 by individual mouse.

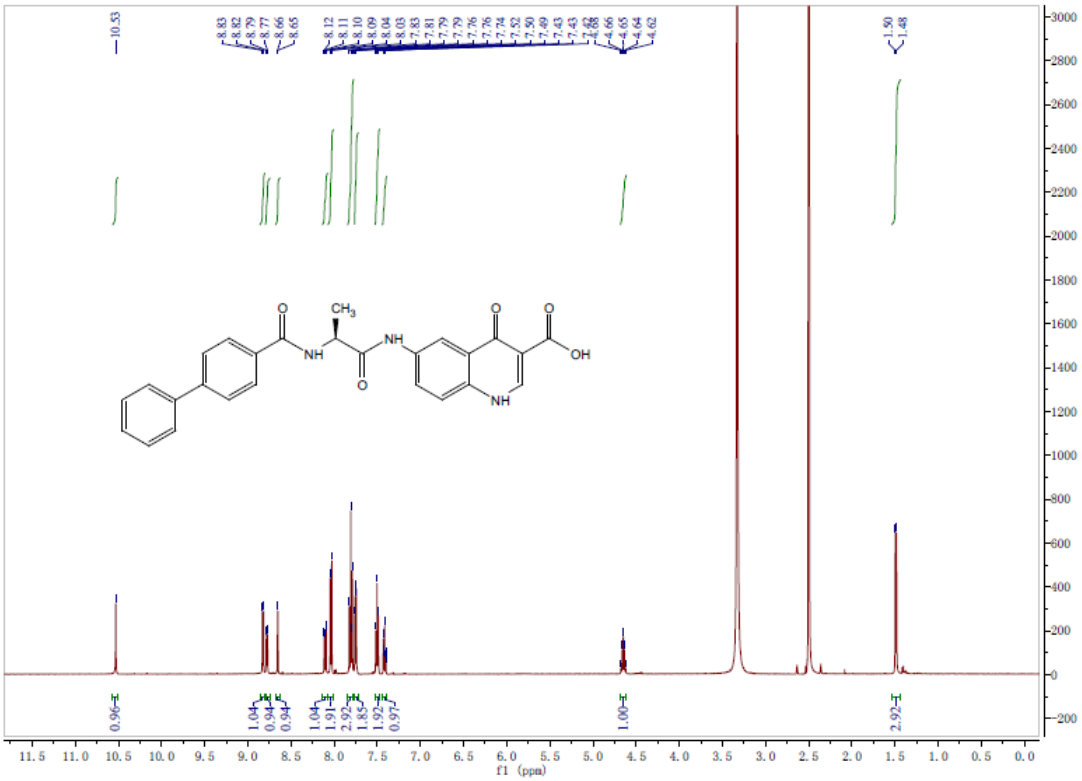


Supplemental Methods Figure 4. $^{1}$H-NMR spectra of L-1

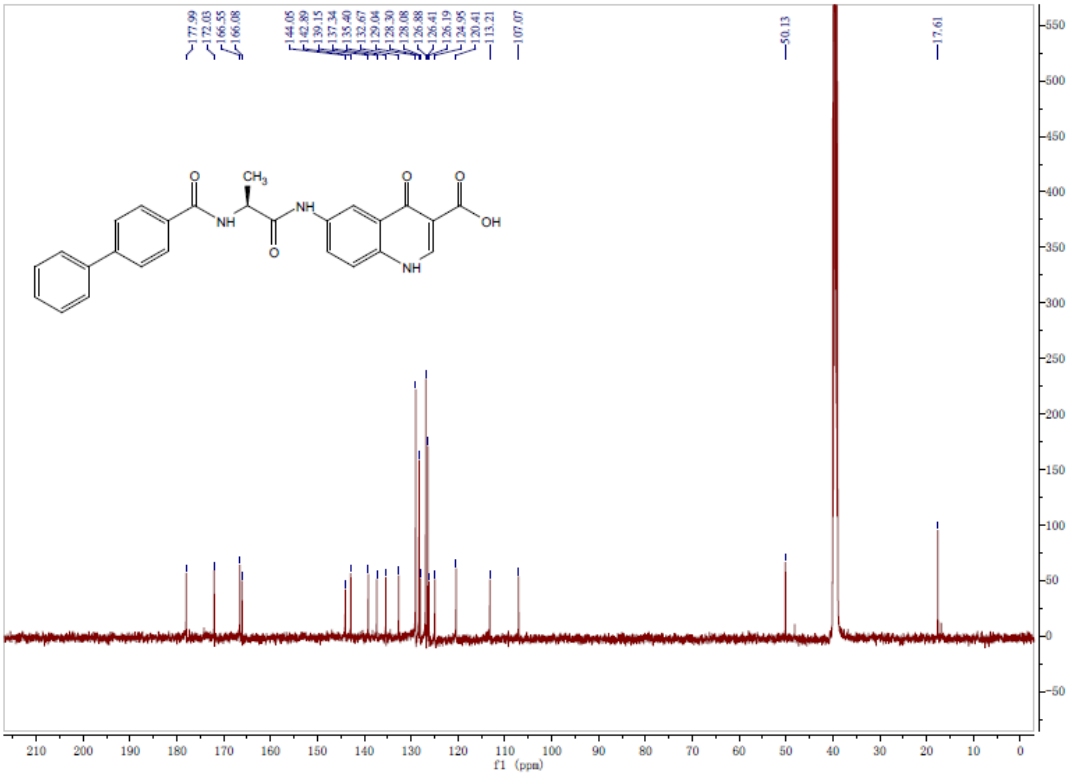


Supplemental Methods Figure 5. $^{13}$C-NMR spectra of L-1

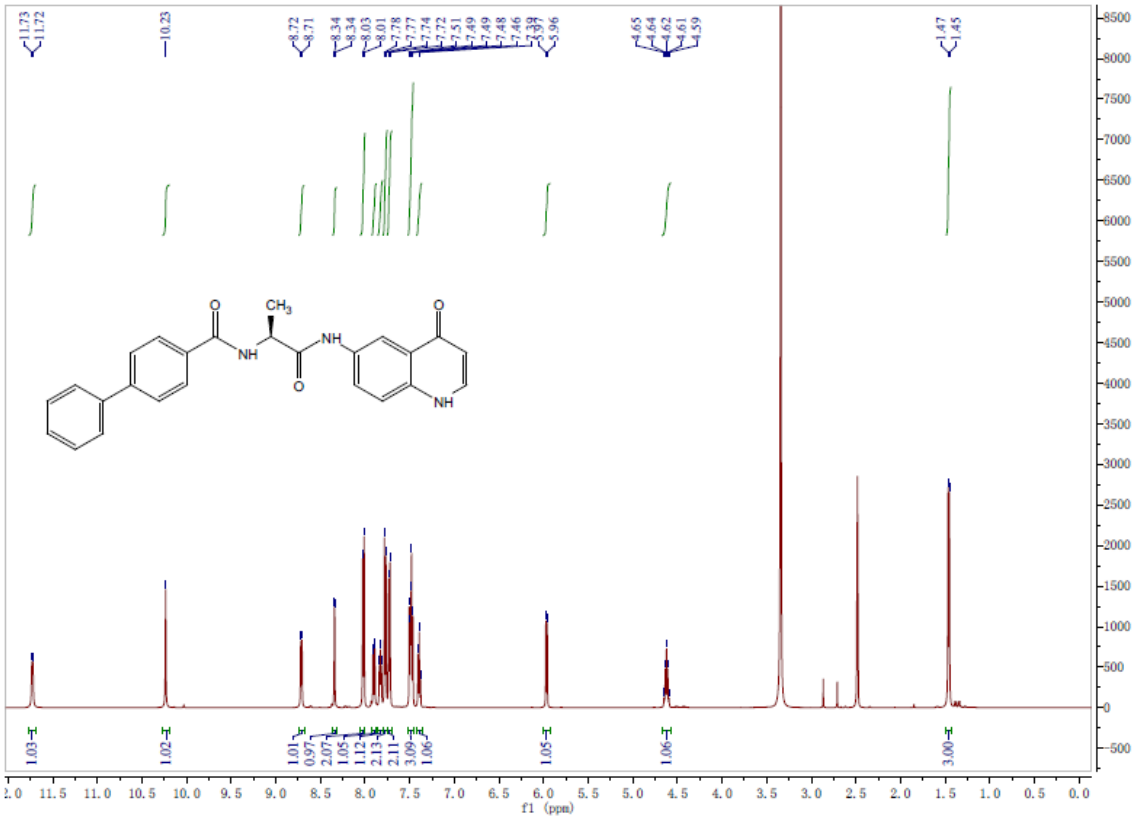


Supplemental Methods Figure 6. $^{1}$H-NMR spectra of L-17

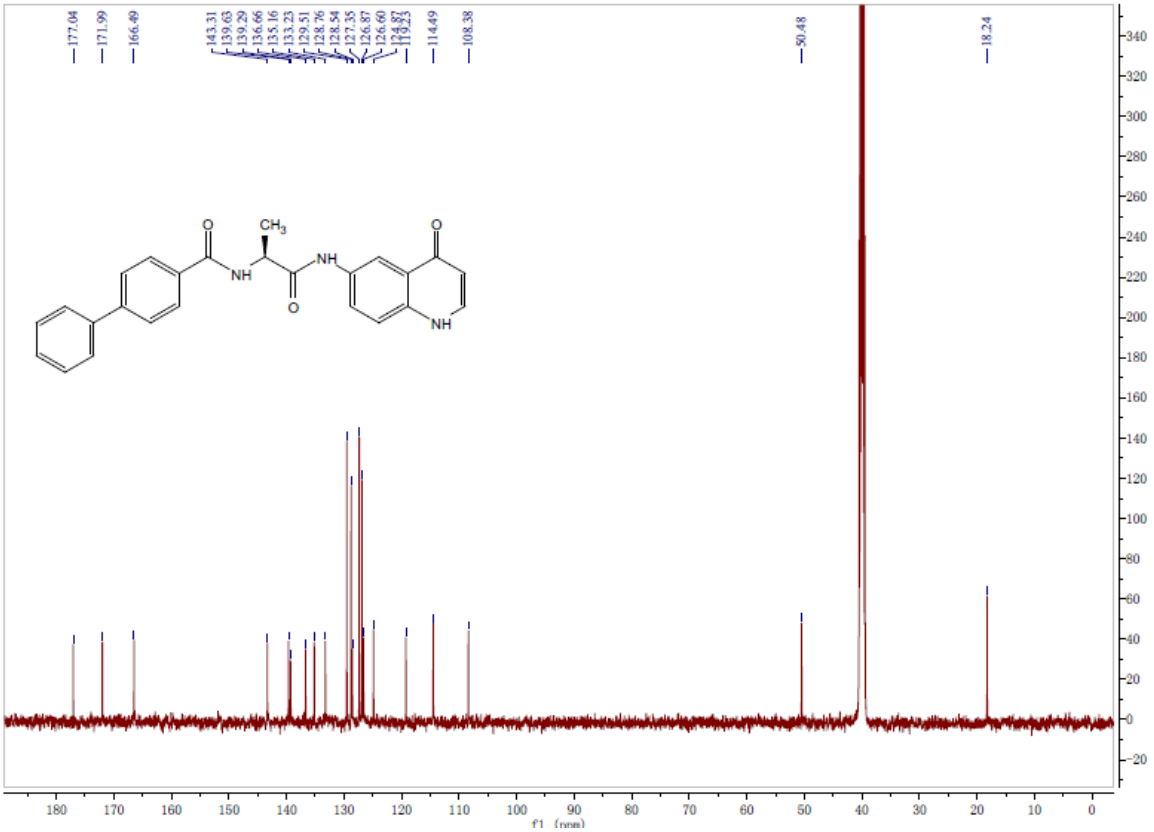


Supplemental Methods Figure 7. $^{13}$C-NMR spectra of L-17

**Supplemental Methods: Antibody Lists**

Supplemental Methods Table 2: Mouse Tumor Immune Profiling Panel

| Metal | Mass | Antigen | Surface | Intracellular | Clone | Titration | Source | Custom |
|---|---|---|---|---|---|---|---|---|
| Pr | 141 | Ly6G | x | | 1A8 | 1:50 | Fluidigm | |
| Ce | 142 | CD11c | x | | N418 | 1:100 | Fluidigm | |
| Nd | 143 | ICOS | x | | C398.4A | 1:100 | Fluidigm | |
| Nd | 145 | CD69 | x | | H1.2F3 | 1:100 | Fluidigm | |
| Nd | 146 | F4_80 | x | | BM8 | 1:100 | Fluidigm | |
| Nd | 148 | CD11b | x | | M1/70 | 1:100 | Fluidigm | |
| Sm | 149 | CD19 | x | | 6D5 | 1:100 | Fluidigm | |
| Nd | 150 | Ly6C | x | | HK1.4 | 1:100 | Fluidigm | |
| Eu | 151 | CD25 | x | | 3C7 | 1:100 | Fluidigm | |
| Sm | 152 | CD3 | x | | 145-2C11 | 1:50 | Fluidigm | |
| Eu | 153 | PDL1 | x | | 10F.9G2 | 1:100 | Fluidigm | |
| Sm | 154 | CTLA4 | x | x | UC10-4B9 | 1:100 | Fluidigm | |
| Gd | 156 | BTLA | x | | 6F7 | 1:100 | Fluidigm | |
| Dy | 158 | CXCR3 | x | | CXCR3-173 | 1:50 | Biolegend | x |
| Tb | 159 | PD1 | x | | 29F.1A12 | 1:100 | Fluidigm | |
| Gd | 160 | CD5 | x | | 53-7.3 | 1:100 | Fluidigm | |
| Dy | 161 | CD40 | x | | HM40-3 | 1:50 | Fluidigm | |
| Dy | 163 | CD27 | x | | LG.3A10 | 1:200 | Biolegend | x |
| Dy | 164 | CD62L | x | | MEL-14 | 1:100 | Fluidigm | |
| Ho | 165 | Foxp3 | | x | FJK-16s | 1:33 | Fluidigm | |
| Er | 166 | RORgt | | x | B2D | 1:50 | Thermo Fisher Scientific | x |
| Er | 167 | KLRG1 | x | | 2F1 | 1:100 | Tonbo | x |
| Er | 168 | CD8 | x | | 53-6.7 | 1:50 | Fluidigm | |
| Er | 170 | CD161 | x | | PK136 | 1:50 | Fluidigm | |
| Yb | 171 | CD44 | x | | IM7 | 1:100 | Fluidigm | |
| Yb | 172 | CD4 | x | | RM4-5 | 1:200 | Fluidigm | |
| Yb | 173 | GZMB | | x | GB11 | 1:100 | Fluidigm | |
| Yb | 174 | Lag3 | x | | C9B7W | 1:100 | Fluidigm | |
| Yb | 176 | B220 | x | | RA3-6B2 | 1:100 | Fluidigm | |

Supplemental Methods Table 3: Mouse Phospho-Profiling Panel

| Metal | Mass | Antigen | Surface | Intracellular | Clone | Titration | Source | Custom |
|---|---|---|---|---|---|---|---|---|
| Dy | 144 | CD247 Y142 | | x | K25-407.69 | 1:100 | BD Biosciences | x |
| Nd | 145 | CD69 | x | | H1.2F3 | 1:100 | Fluidigm | |
| Sm | 149 | CD19 | x | | 6D5 | 1:100 | Fluidigm | |
| Eu | 151 | CD25 | x | | 3C7 | 1:100 | Fluidigm | |
| Sm | 152 | CD3 | x | | 145-2C11 | 1:50 | Fluidigm | |
| Eu | 153 | PDL1 | x | | 10F.9G2 | 1:100 | Fluidigm | |
| Sm | 154 | CTLA4 | x | x | UC10-4B9 | 1:100<br>1:500 | Fluidigm | |
| Gd | 156 | p38 T180/Y182 | | x | D3F9 | 1:75 | Fluidigm | |
| Dy | 158 | pLAT Y226 | | x | J96-1238.58.93 | 1:50 | BD Biosciences | x |
| Tb | 159 | PD1 | x | | 29F.1A12 | 1:100 | Fluidigm | |
| Gd | 160 | CD5 | x | | 53-7.3 | 1:100 | Fluidigm | |
| Dy | 162 | Lck Y505 | | x | 4 | 1:100 | Fluidigm | |
| Dy | 163 | MEK1 T202/Y204 | | x | 20A | 1:100 | BD Biosciences | x |
| Dy | 164 | CD62L | x | | MEL-14 | 1:100 | Fluidigm | |
| Er | 166 | Lck Y394 | | x | D49G4 | 1:50 | Cell Signaling | x |
| Er | 167 | ERK T202/Y204 | | x | D13.14.4E | 1:100 | Fluidigm | |
| Er | 168 | CD8 | x | | 53-6.7 | 1:50 | Fluidigm | |
| Tb | 169 | Zap70 Y493 | | x | Polyclonal | 1:50 | Cell Signaling | x |
| Er | 170 | CD161 | x | | PK136 | 1:50 | Fluidigm | |
| Yb | 171 | CD44 | x | | IM7 | 1:100 | Fluidigm | |
| Yb | 172 | Ki67 | | x | B56 | 1:200 | Fluidigm | |
| Yb | 173 | GZMB | | x | GB11 | 1:100 | Fluidigm | |
| Yb | 174 | Lag3 | x | | C9B7W | 1:100 | Fluidigm | |
| Lu | 175 | CD127 | x | | A7R34 | 1:100 | Fluidigm | |
| Yb | 176 | B220 | x | | RA3-6B2 | 1:100 | Fluidigm | |

Supplemental Methods Table 4: Human Phospho-Profiling Panel

| Metal | Mass | Antigen | Surface | Intracellular | Clone | Titration | Source | Custom |
|---|---|---|---|---|---|---|---|---|
| Nd | 142 | CD19 | x | | HIB19 | 1:100 | Fluidigm | |
| Dy | 144 | CD247 Y142 | | x | K25-407.69 | 1:100 | BD Biosciences | x |
| Nd | 145 | CD4 | x | | RPA-T4 | 1:200 | Fluidigm | |
| Nd | 146 | CD8a | x | | RPA-T8 | 1:200 | Fluidigm | |
| Nd | 148 | CD16 | x | | 3G8 | 1:200 | Fluidigm | |
| Sm | 149 | CD25 | x | | 2A3 | 1:400 | Fluidigm | |
| Nd | 150 | OX40 | x | | ACT35 | 1:200 | Fluidigm | |
| Eu | 151 | CD2 | x | | TS1/8 | 1:400 | Fluidigm | |
| Gd | 155 | PD1 | x | | EH12.2H7 | 1:200 | Fluidigm | |
| Dy | 158 | pLAT Y226 | | x | J96-1238.58.93 | 1:50 | BD Biosciences | x |
| Tb | 159 | PD1 | x | | 29F.1A12 | 1:100 | Fluidigm | |
| Dy | 161 | CTLA4 | x | x | 14D3 | 1:200<br>1:500 | Fluidigm | |
| Dy | 162 | Lck Y505 | | x | 4 | 1:100 | Fluidigm | |
| Dy | 163 | MEK1 T202/Y204 | | x | 20A | 1:100 | BD Biosciences | x |
| Ho | 165 | CD45RO | x | | UCHL1 | 1:100 | Fluidigm | |
| Er | 166 | Lck Y394 | | x | D49G4 | 1:50 | Cell Signaling | x |
| Er | 167 | ERK T202/Y204 | | x | D13.14.4E | 1:100 | Fluidigm | |
| Tb | 169 | Zap70 Y493 | | x | Polyclonal | 1:50 | Cell Signaling | x |
| Yb | 171 | Zap70 Y319 | | x | 17a | 1:100 | Fluidigm | |
| Yb | 172 | Ki67 | | x | B56 | 1:200 | Fluidigm | |
| Yb | 173 | GZMB | | x | GB11 | 1:100 | Fluidigm | |
| Lu | 175 | Lag3 | x | | 11C3C65 | 1:100 | Fluidigm | |
| Yb | 176 | CD127 | x | | A019D5 | 1:100 | Fluidigm | |

Supplemental Methods Table 5: Mouse Macrophage Focused Panel

| Metal | Mass | Antigen | Surface | Intracellular | Clone | Titration | Source | Custom |
|---|---|---|---|---|---|---|---|---|
| Pr | 141 | LY6G | x | | 1A8 | 1:50 | Fluidigm | |
| Ce | 142 | CD11C | x | | N418 | 1:100 | Fluidigm | |
| Nd | 143 | CD69 | x | | H1.2F3 | 1:400 | Fluidigm | |
| Nd | 144 | B220 | x | | RA3-6B2 | 1:400 | Fluidigm | |
| Nd | 145 | CD4 | x | | RM4-5 | 1:400 | Fluidigm | |
| Nd | 146 | F480 | x | | BM8 | 1:100 | Fluidigm | |
| Sm | 147 | CD45 | x | | 30-F11 | 1:100 | Fluidigm | |
| Nd | 148 | CD11B | x | | M1/70 | 1:100 | Fluidigm | |
| Sm | 149 | CD19 | x | | 6D5 | 1:100 | Fluidigm | |
| Nd | 150 | LY6C | x | | HK1.4 | 1:100 | Fluidigm | |
| Eu | 151 | CD25 | x | | 3C7 | 1:100 | Fluidigm | |
| Sm | 152 | CD3E | x | | 145-2C11 | 1:50 | Fluidigm | |
| Eu | 153 | PDL1 | x | | 10F.9G2 | 1:100 | Fluidigm | |
| Gd | 155 | IRF4 | | x | 3E4 | 1:100 | Fluidigm | |
| Tb | 159 | PD1 | x | | 29F.1A12 | 1:100 | Fluidigm | |
| Dy | 161 | CD40 | x | | HM40-3 | 1:50 | Fluidigm | |
| Dy | 162 | KI67 | | x | B56 | 1:200 | Fluidigm | |
| Dy | 163 | CD86 | x | | GL-1 | 1:400 | Biolegend | x |
| Dy | 164 | CD62L | x | | MEL-14 | 1:100 | Fluidigm | |
| Er | 168 | CD8A | x | | 53-6.7 | 1:50 | Fluidigm | |
| Tm | 169 | CD206 | | x | C068C2 | 1:100 | Fluidigm | |
| Er | 170 | NK1.1 | x | | PK136 | 1:50 | Fluidigm | |
| Yb | 171 | CD44 | x | | IM7 | 1:100 | Fluidigm | |
| Yb | 172 | PRF1 | | x | OMAKD | 1:50 | Fluidigm | |
| Lu | 175 | CD80 | x | | 16-10A1 | 1:400 | Biolegend | x |
| Bi | 209 | IAIE | x | | M5/114.15.2 | 1:100 | Fluidigm | |

Supplemental Methods Table 6: Barcoding and Ancillary Markers

| Metal | Mass | Antigen | Surface | Intracellular | Clone | Titration | Source | Custom |
|---|---|---|---|---|---|---|---|---|
| Y | 89 | Mouse CD45 | x | | 30-F11 | 1:100 | Fluidigm | |
| Y | 89 | Human CD45 | x | | HI30 | 1:100 | Fluidigm | |
| Rh | 103 | Cell-ID | | x | NA | 1:1000 | Fluidigm | |
| Pd | 104-110 | Dead | | x | NA | 500nM | Sigma | |
| Cd | 112 | Mouse CD45 | x | | 30-F11 | 1:200 | Biolegend | x |
| Cd | 112 | Mouse CD29 | x | | HMβ1-1b | 1:200 | Biolegend | x |
| Cd | 112 | Mouse CD98 | x | | RL388 | 1:200 | Biolegend | x |
| In | 113 | Mouse CD45 | x | | 30-F11 | 1:200 | Biolegend | x |
| In | 113 | Mouse CD29 | x | | HMβ1-1b | 1:200 | Biolegend | x |
| In | 113 | Mouse CD98 | x | | RL388 | 1:200 | Biolegend | x |
| In | 113 | Human CD45 | x | | HI30 | 1:200 | Biolegend | x |
| Cd | 114 | Mouse CD45 | x | | 30-F11 | 1:200 | Biolegend | x |
| Cd | 114 | Mouse CD29 | x | | HMβ1-1b | 1:200 | Biolegend | x |
| Cd | 114 | Mouse CD98 | x | | RL388 | 1:200 | Biolegend | x |
| In | 115 | Mouse CD45 | x | | 30-F11 | 1:200 | Biolegend | x |
| In | 115 | Mouse CD29 | x | | HMβ1-1b | 1:200 | Biolegend | x |
| In | 115 | Mouse CD98 | x | | RL388 | 1:200 | Biolegend | x |
| In | 115 | Human CD45 | x | | HI30 | 1:200 | Biolegend | x |
| Cd | 116 | Mouse CD45 | x | | 30-F11 | 1:200 | Biolegend | x |
| Cd | 116 | Mouse CD29 | x | | HMβ1-1b | 1:200 | Biolegend | x |
| Cd | 116 | Mouse CD98 | x | | RL388 | 1:200 | Biolegend | x |
| Pt | 194 | Mouse CD45 | x | | 30-F11 | 1:100 | Biolegend | x |
| Pt | 194 | Human CD45 | x | | HI30 | 1:100 | Biolegend | x |
| Pt | 198 | Mouse CD45 | x | | 30-F11 | 1:100 | Biolegend | x |
| Pt | 198 | Human CD45 | x | | HI30 | 1:100 | Biolegend | x |

Supplemental Methods Table 7: Flow Cytometry Antibodies

| Panel | Channel | Antigen | Surface | Intracellular | Clone | Titration | Source |
|---|---|---|---|---|---|---|---|
| Tumor infiltrating T cells | FITC | CD45 | x | | 30-F11 | 1:100 | Biolegend |
| Tumor infiltrating T cells | Near IR | Live/dead | | x | NA | 1:1000 | Invitrogen |
| Tumor infiltrating T cells | PB | CD4 | x | | RM4-5 | 1:100 | Biolegend |
| Tumor infiltrating T cells | BV510 | CD8 | x | | 53-6.7 | 1:100 | BD Biosciences |
| Transcriptional Factors | BV421 | CD3 | x | | 17A2 | 1:100 | BD Biosciences |
| Transcriptional Factors | BV605 | CD4 | x | | RM4-5 | 1:100 | BD Biosciences |
| Transcriptional Factors | BV786 | CD8 | x | | 53-6.7 | 1:100 | BD Biosciences |
| Transcriptional Factors | PE | EOMES | | x | Dan11mag | 1:100 | Thermo Fisher |
| Transcriptional Factors | APC | Tbet | | x | 4B10 | 1:100 | Biolegend |
| Co-culture | PB | CD3 | x | | 145-2C11 | 1:800 | Biolegend |
| Co-culture | BV605 | CD4 | x | | RM4-5 | 1:200 | Biolegend |
| Co-culture | BV786 | CD8 | x | | 53-6.7 | 1:200 | Biolegend |
| Co-culture | PE-DAZ594 | CD44 | x | | IM7 | 1:1000 | Biolegend |
| Co-culture | PerCP/Cy5.5 | CD69 | x | | H1.2F3 | 1:100 | Biolegend |
| Co-culture | PE-Cy7 | Granzyme B | | x | NGZB | 1:100 | Biolegend |
| Co-culture | APC | IFNγ | | x | XMG1.2 | 1:100 | Biolegend |
| Co-culture | AF700 | IL2 | | x | JES6-5H4 | 1:100 | Biolegend |

## References

1. Al-As'ad, R. M., El-Abadelah, M. M., Sabri, S. S., Zahra, J. A. & Voelter, W. Synthesis of 6-ethyl-1,2,9-trioxopyrrolo[3,2-f ]quinoline-8-carboxylic acid. *Zeitschrift fur Naturforsch. - Sect. B J. Chem. Sci.* **68**, 700–706 (2013).